nature communications

Article

https://doi.org/10.1038/s41467-025-57970-9

Altermagnetism from coincident Van Hove singularities: application to κ-Cl

Received: 26 July 2024

Accepted: 8 March 2025

Published online: 26 March 2025

Check for updates

Yue Yu [1] ✉, Han Gyeol Suh[1], Mercè Roig [2] & Daniel F. Agterberg [1]

Realizing two-dimensional (2D) altermagnets is important for spintronics applications. Here we propose a microscopic template for stabilizing 2D altermagnetism through Van Hove singularities that are coincident in both energy and momentum. These coincident Van Hove singularities are a generic consequence of non-symmorphic symmetries in nine 2D space groups. Due to nontrivial symmetry properties of the Hamiltonian, these coincident Van Hove singularities allow new hopping interactions between the Van Hove singularities that do not appear in analogous Van Hove singularity based patch models for cuprates and graphene. We show these new interactions can give rise to various weak coupling, and BCS-based instabilities, including altermagnetism, nematicity, inter-band d-wave superconductivity, and orbital altermagnetic order. We apply our results to quasi-2D organic κ-Cl in which altermagnetism is known to appear.

Altermagnetism, distinct from ferromagnetism and antiferromagnetism, exhibits zero net magnetization with momentum-dependent collinear spin textures[1–13]. Analogous to unconventional superconductors, it establishes a profound connection between magnetism and topology, hosting nonzero Berry curvature for anomalous Hall transport[2,14–21]. The momentum-dependent spin splitting serves as a intrinsic platform for spin-current coupling[22], enabling practical control in spin devices through the application of magnetic fields[23,24], electrical currents[1,25–29], strain[30–34], torque[35,36], and heat[37,38]. When coupled with superconductors, altermagnetism can induce intriguing phenomena[39–41], such as the Fulde-Ferrell-Larkin-Ovchinnikov (FFLO) state[42,43] and new platforms for enabling Majorana particles[44].

As demonstrated through density functional theory (DFT)-based Hartree-Fock calculations[3], the random phase approximation[45], and analysis of Fermi surface Pomeranchuk instabilities[3,46], altermagnetism is believed to be stabilized through strong on-site Coulomb interactions. Searches for this strong coupling instability form the basis for identifying new altermagnetic materials. In principle, in 2D, Van Hove singularities offer a weak coupling route towards stabilizing altermagnetism. Van Hove singularities are saddle points in the energy dispersion and induce a logarithmic divergence in the 2D density of states. Tuning the chemical potential across such singularities results in divergent susceptibilities, signaling an instability into a variety of possible competing orders that have been examined in cuprates, graphene, and Kagome metals[47–62]. However, in these applications, altermagnetism is not one of these competing orders, suggesting that this route is not viable for stabilizing this state. Indeed, the closest relative to altermagnetism that has been found is a non-collinear variant that appears only for fine-tuned higher-order Van Hove singularities[62].

In contrast to the strong-coupling mechanisms typically examined with RPA-like approaches, here we identify a weak-coupling mechanism based on usual 2D logarithmic Van-Hove singularities that stabilize altermagnetism. Two ingredients are key to realizing this mechanism. The first is the existence of a pair of Van Hove singularities that are coincident in both energy and momentum. The second, which does not hold for all coincident Van Hove singularites, is a specific symmetry property of the Hamiltonian, which give rise to a new hopping interaction between these Van Hove singularities. This hopping interaction does not appear in Van Hove-based patch models for cuprates[50–53] and graphene[47–49,62] where it is forbidden by translation invariance. Both ingredients are a generic consequence of non-symmorphic symmetries that exist in nine 2D space groups, when spin-orbit coupling is neglected. Furthermore, unlike the Van Hove driven spin density wave transitions that occur in cuprate[50–53],

[1]Department of Physics, University of Wisconsin-Milwaukee, Milwaukee, Wisconsin 53201, USA. [2]Niels Bohr Institute, University of Copenhagen, DK-2100 Copenhagen, Denmark. ✉e-mail: yu36@uwm.edu

graphene[47–49,62], and Kagome metal[54] patch models, our altermagnetic mechanism does not require nesting or near-nesting of the bands. Instead, it is based on the BCS instability, which typically yields only a superconducting instability for the other Van Hove singularity scenarios. Our analysis also stabilizes other orders including interband d-wave superconductivity, nematicity, and orbital altermagnetism. To be concrete, we apply our analysis to the organic material κ-Cl where an altermagnetic state is believed to occur.

Results

Coincident Van Hove singularities

The phase diagram of the quasi-2D orthorhombic organic compound κ-$(ET)_2Cu[N(CN)_2]Cl$ (κ-Cl, 2D layer group L25 (pba2)) shares similarities with cuprates[63], exhibiting unconventional superconductivity adjacent to magnetism under pressure[64–66] and anion substitution[67–74]. Previous theoretical studies, largely based on strong coupling RPA-like calculations, reveal superconducting and altermagetic states[75–77]. DFT calculations reveal a Van Hove singularity at the S = (π, π) point[78]. Recently, considerable hole-doping has been achieved in κ-Cl[79]. As the Van Hove singularity is approached, a substantial reduction in spectral weight is observed, revealing the importance of electronic correlations[79]. Here we show that this Van Hove singularity consists of a pair of Van Hove singularities that are coincident in both energy and momentum, and also satisfies the symmetry conditions that allow the new hopping interaction mentioned above. We also show that in the vicinity of the Van Hove singularity, interactions that fall outside of RPA-like approaches drive a weak-coupling instability to altermagnetism and other novel states.

For pedagogical purposes, we start with a tight-binding Hamiltonian. A general group theory analysis can be found later. κ-Cl has four ET molecules per unit cell, forming two molecule-dimers (Fig. 1) at positions: $(r_1, r_2) = \{(0, 0), (1/2, 1/2)\}$. As a minimal model capturing the coincident Van Hove singularities, we consider one orbital on each dimer position. The Pauli matrices τ_i act in dimer (or sublattice) space and the Pauli matrices σ_i act in spin space. While spin-orbit coupling (SOC) is negligible[1,78], the normal state tight-binding Hamiltonian is:

$$H = 2t_1\cos k_x + 2t_2\cos k_y + 4t_3\cos k_x\cos k_y + 4t_4\cos\frac{k_x}{2}\cos\frac{k_y}{2}\tau_x + t_5\sin k_x\sin k_y\tau_z - \mu. \quad (1)$$

Here, τ_x term describes inter-sublattice hopping (thick black arrows in Fig. 1). τ_z term captures the difference in intra-sublattice hopping between (1, 1) and (1, − 1) directions (solid/dashed red arrows in Fig. 1), which is opposite on the two sublattices. Each band is doubly degenerate, consisting of spin-up and down states. Due to the nonsymmorphic symmetries, the band without SOC is 4-fold degenerate at the entire Brillouin zone boundary $k_x = \pi$ and $k_y = \pi$[80]. Near the Brillouin zone corner S=(π, π), where the coincident Van Hove singularities appear, we obtain the kp Hamiltonian:

$$H(\pi + k_x, \pi + k_y) = t_x k_x^2 + t_y k_y^2 + k_x k_y(t_4\tau_x + t_5\tau_z) - \tilde{\mu}, \quad (2)$$

with $\tilde{\mu} = \mu + 2t_1 + 2t_2 - 4t_3$, t_x = (t_1 − $2t_3$), and t_y = (t_2 − $2t_3$). This expansion reveals a central property of all the theories we examine here, both the operators τ_x and τ_z are multiplied by the momentum function k_xk_y. Since the Hamiltonian must be invariant under all orthorhombic symmetries, this implies that both τ_x and τ_z share the same symmetry as k_xk_y at the S point. A group theory analysis (given in detail later) applied to the momentum points and 2D and 3D space groups in Table 1 reveals that the kp-theory of Eq. (2) also appears in these cases and has the most general form allowed by symmetry (for the 3D groups, a term $a_zk_z^2$ is also allowed, and the physics discussed here occurs in the quasi-2D limit, where a_z is small relative to t_x and t_y). The other non-trivial sublattice operator τ_y is time-reversal odd, but invariant under all crystal symmetries. τ_y can only appear in a Hamiltonian multiplied by spin-1/2 operators[80] as a SOC term. Here we ignore SOC and include a discussion of its effects in the appendix.

The resulting dispersions of the two bands are

$$E_{1,2} = t_xk_x^2 + t_yk_y^2 \pm \sqrt{t_4^2 + t_5^2}k_xk_y - \tilde{\mu}. \quad (3)$$

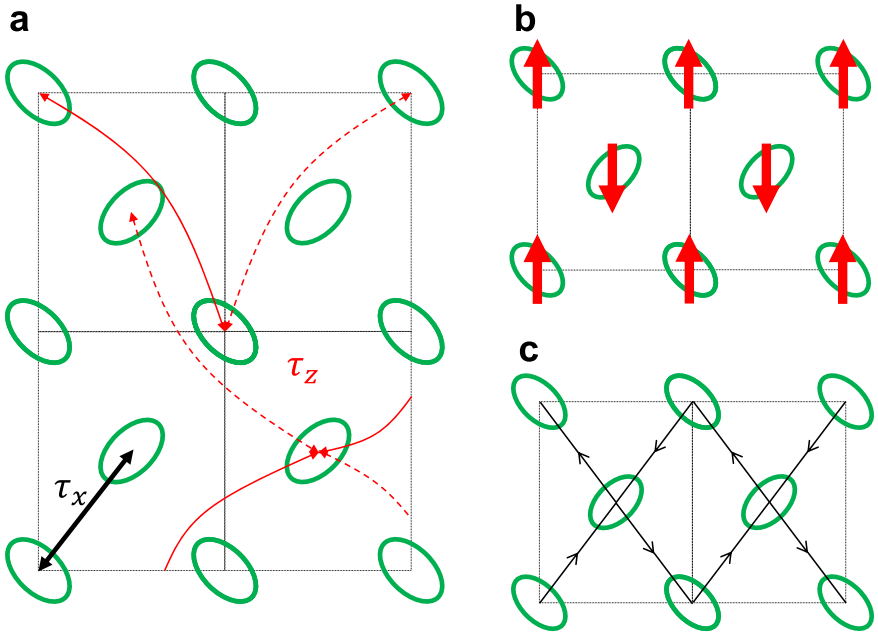

Fig. 1 | Crystal structure. a Hopping parameters. **b** Altermagnet where arrows represent spins. **c** Orbital altermagnet where arrows represent currents (even-parity current loop order). We name this state an orbital altermagnet since the local moments induced by the current loops form an altermagnet (which has the same symmetries as the altermagnet depicted in (**b**)).

Table 1 | 2D layer groups and 3D space groups[87,88] hosting the kp Hamiltonian in Eq.(2) at quadratic level

2D	L17(p2_1/b11), L21(p2_12_12), L25(pba 2) L44(pbam), L54(p42_12), L56(p4bm) L58(p $\bar{4}2_1$ m), L60(p $\bar{4}$ b2), L63(p4/mbm)
3D	18(P2_12_12)R&S, 19(P$2_12_12_1$)S&T (k_yk_z)&$U(k_xk_z)$ 55(Pbam)R&S, 56(Pccn)R, 58(Pnnm)S 62(Pnma)U, 90(P42_12)M&A, 92(P4_12_12)M 94(P4_22_12)M&A, 96(P4_32_12)M, 127(P4/mbm)M&A 128(P4/mnc)M, 135(P4_2/mbc)M, 136(P4_2/mnm)M 138(P4_2/ncm)A, 212(P4_32)M, 213(P4_132)M

For 2D layer groups, the kp Hamiltonian is centered at the (π, π) point. For 3D space groups, the corresponding high-symmetry points are included. In 19T(19U), the coefficients of $\tau_{x,z}$ terms are $k_yk_z(k_xk_z)$ instead of k_xk_y.

The saddle point conditions for these two dispersions are the same: $t_4^2+t_5^2+(t_x-t_y)^2>(t_x+t_y)^2$. Consequently, each band hosts a Van Hove singularity at the band crossing point $S=(\pi,\pi)$.

In the following, we work in the band basis for which the kp Hamiltonian, Eq. (2) is diagonal. To diagonalize the kp Hamiltonian, we take a k-independent unitary transformation $u=\cos(\theta/2)I-i\sin(\theta/2)\tau_y$ where $\cos\theta=t_5/\sqrt{t_4^2+t_5^2}$. In the band basis, $\tilde{\tau_y}$ is unchanged from τ_y in the sublattice basis. $\tilde{\tau_x}$ and $\tilde{\tau_z}$ in the band basis are linear combinations of τ_x and τ_z, with $\tilde{\tau_x}=\cos\theta\tau_x-\sin\theta\tau_z$ and $\tilde{\tau_z}=\sin\theta\tau_x+\cos\theta\tau_z$. Since $\tau_{x,z}$ have the same symmetry and θ is a constant, $\widetilde{\tau_{x,z}}$ should remain the same symmetry as k_xk_y. As interactions can be constructed from multiplying Fermionic bilinears with the same symmetry, this indicates the existence of a new interaction term with respect to kp theories in which τ_x and τ_z have different symmetries.

Patch model and interactions

The coincident Van Hove singularities provide a novel platform to study strongly interacting fermions and a natural mechanism for stabilizing 2D altermagnetism. To understand this, it is useful to consider a patch model[50]. Here, the density of states (DOS) of each band is approximated as a patch situated solely at the Van Hove point. With a Van Hove singularity on each band, we end up with two DOS patches located at the same point: (π, π), as shown in Fig. 2. This patch model has similarities with that examined for cuprates. For cuprates, there are also two Van Hove singularities, but these Van Hove singularities are not coincident and appear at the two distinct momenta (0, π) and (π, 0). The key difference between patch models for coincident Van Hove points and those for the cuprates is in the interactions allowed by symmetry. Both models contain the standard interactions g_1, g_2, g_3, and g_4. However, our coincident Van Hove patch model contains a new hopping interaction, g_5, shown in Fig. 3

This g_5-interaction involves a hopping between the two bands (DOS patches) which, due to momentum conservation, is permissible only when two patches coincide. The existence of coincident Van Hove singularities is not sufficient for the existence of the g_5 interaction. Additionally, the Hamiltonian must satisfy the symmetry condition discussed just below Eq. 2 that $\tilde{\tau_x}$ and $\tilde{\tau_z}$ have the same symmetry. To demonstrate this, we use Cooper pair operators to derive the g_5 interaction. Cooper pair operators are convenient since they automatically encode the Pauli exclusion principle. The interactions in Fig. 3 involve annihilating two electrons (a Cooper pair) from the left and then creating another Cooper pair with the same symmetry to the right. For g_5, the corresponding Cooper pairs are $\tilde{\tau_x}i\sigma_y$: $\Delta_{xy,1}=c_{2\downarrow}c_{1\uparrow}+c_{1\downarrow}c_{2\uparrow}$ and $\tilde{\tau_z}i\sigma_y$: $\Delta_{xy,2}=c_{1\downarrow}c_{1\uparrow}-c_{2\downarrow}c_{2\uparrow}$ (here 1 and 2 in Fermionic operators label the bands). Since these two Cooper pairs share the same symmetry, the interaction $g_5\Delta^\dagger_{xy,1}\Delta_{xy,2}$ is symmetry

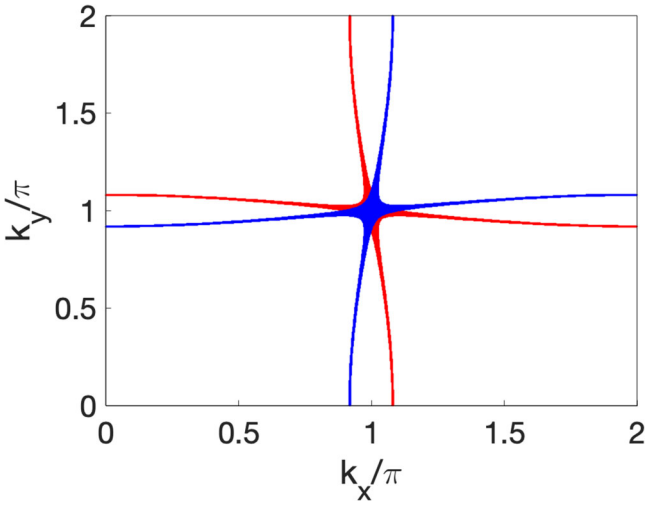

Fig. 2 | Density of states is concentrated near the band crossing point (π, π), where the two bands are shown in different colors. In the patch model, states on the red band are replaced by a single point at (π, π), while states on the blue band are replaced by another point at (π, π). Here, we take $t_1=t_2=t_5=1$, $t_3=0$, $t_4=8$, and $\mu=-4$. 2000^2 points are sampled, and states with energy ($|E|<0.1$) are plotted.

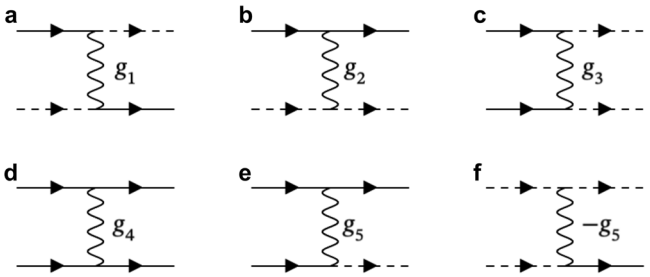

Fig. 3 | Allowed interactions for two coincident patches. a–f The exchange interaction g_1, inter-patch Hubbard interaction g_2, pair-hopping interaction g_3, intra-patch Hubbard interaction g_4, and the new hopping interaction g_5. Here, upper propagators are for spin-up, while lower ones are for spin-down. Solid& dashed lines label bands 1 and 2.

allowed. If the $\tilde{\tau_x}$ and $\tilde{\tau_z}$ operators had different symmetries, this interaction would be symmetry forbidden. Expanding $g_5\Delta^\dagger_{xy,1}\Delta_{xy,2}$ yields

$$H^{int}_{g_5}=g_5(c_{2\downarrow}c_{1\uparrow}+c_{1\downarrow}c_{2\uparrow})^\dagger(c_{1\downarrow}c_{1\uparrow}-c_{2\downarrow}c_{2\uparrow})+h.c. \quad (4)$$

In the two g_5 panels in Fig. 3, the two input electrons from the left annihilates the Cooper pair $\Delta_{xy,2}$, and the two output electrons to the right creates the Cooper pair $\Delta^\dagger_{xy,1}$. The sign difference on the two bands in $\Delta_{xy,2}$ results in the sign difference between the two $\pm g_5$ panels.

The g_5 interaction can be generated by an on-site Hubbard interaction after transforming to the band basis, so its magnitude can be large. In particular, for the interaction

$$H_{\rm int}=U\sum_m n_{m\uparrow}n_{m\downarrow}, \quad (5)$$

where m denotes the sublattice index, we find its components in the band basis (denoted by g_i^0): $g_1^0=g_2^0=g_3^0=(U/2)\sin^2\theta$, $g_3^0+g_4^0=U$, $g_4^0-g_3^0=U\cos^2\theta$, and $g_5^0=(U/2)\sin\theta\cos\theta$. Recall $\cos\theta\equiv t_5/\sqrt{t_4^2+t_5^2}$, the existence of g_5 thus requires both $k_xk_y(t_4\tau_x+t_5\tau_z)$ terms

in the dispersion. In single-band cuprates, even if we fold the Brillouin zone such that the two Van Hove singularities coincide, g_5 will still vanish as it corresponds to $\theta = \pi/2$.

When the chemical potential is tuned close to the Van Hove singularity, the enhancement in the density of states results in substantial corrections to interaction strengths. These corrections originate through the intra- and inter-band particle-particle (χ_{pp}^{intra}, χ_{pp}^{inter}) and particle-hole (χ_{ph}^{intra}, χ_{ph}^{intra}) susceptibilities for the free fermions[47–61]. Here, these susceptibilities are

$$\begin{aligned}
\chi_{ph}^{intra} &= -\lim_{\mathbf{q}\to 0}\tfrac{1}{N}\textstyle\sum_{\mathbf{k}}\frac{f[E_1(\mathbf{k})]-f[E_1(\mathbf{k}+\mathbf{q})]}{E_1(\mathbf{k})-E_1(\mathbf{k}+\mathbf{q})}\\
\chi_{ph}^{inter} &= -\lim_{\mathbf{q}\to 0}\tfrac{1}{N}\textstyle\sum_{\mathbf{k}}\frac{f[E_1(\mathbf{k})]-f[E_2(\mathbf{k}+\mathbf{q})]}{E_1(\mathbf{k})-E_2(\mathbf{k}+\mathbf{q})}\\
\chi_{pp}^{intra} &= -\lim_{\mathbf{q}\to 0}\tfrac{1}{N}\textstyle\sum_{\mathbf{k}}\frac{f[E_1(-\mathbf{k})]-f(-E_1(\mathbf{k}+\mathbf{q})]}{E_1(-\mathbf{k})+E_1(\mathbf{k}+\mathbf{q})}\\
\chi_{pp}^{inter} &= -\lim_{\mathbf{q}\to 0}\tfrac{1}{N}\textstyle\sum_{\mathbf{k}}\frac{f[E_1(-\mathbf{k})]-f[-E_2(\mathbf{k}+\mathbf{q})]}{E_1(-\mathbf{k})+E_2(\mathbf{k}+\mathbf{q})},
\end{aligned} \tag{6}$$

where $f[E]$ is the Fermi Dirac distribution. The dominant corrections stem from χ_{pp}^{intra}. This is because χ_{pp}^{intra} exhibits the conventional BCS logarithmic divergence multiplied by the logarithmic divergence in the density of states (χ_{pp}^{intra} diverges as $\log^2\Lambda/T$) while other susceptibilities only exhibit the latter and hence diverge as $\log\Lambda/T$. Keeping only the dominant interaction corrections, the one-loop BCS corrections to the interactions are:

$$\begin{aligned}
\Delta g_1 &= -2\chi_{pp}^{intra} g_5^2\\
\Delta g_2 &= -2\chi_{pp}^{intra} g_5^2\\
\Delta g_3 &= -2\chi_{pp}^{intra} g_3 g_4\\
\Delta g_4 &= -\chi_{pp}^{intra}(g_3^2+g_4^2)\\
\Delta g_5 &= -\chi_{pp}^{intra}(g_4-g_3)g_5\\
\rightarrow &\quad \begin{bmatrix} \Delta(g_4+g_3) = -\chi_{pp}^{intra}(g_4+g_3)^2 \\ \Delta(g_4-g_3) = -\chi_{pp}^{intra}(g_4-g_3)^2 \end{bmatrix}.
\end{aligned} \tag{7}$$

Let us start with $g_5 = 0$, then these equations are the same as those found in cuprate patch models[50,52]. Hence, a bare attractive $g_4^0 + g_3^0$ (or $g_4^0 - g_3^0$) enhances itself and gives an intra-band s-wave superconducting $\Delta = i\sigma_y$ (or d-wave superconducting $\Delta = i\tilde{\tau}_z\sigma_y$) instability. For onsite Hubbard interactions and generic θ, we have $g_4^0 > g_3^0 > 0$, causing the BCS correction to suppress these two instabilities.

The g_5-interaction introduces new one-loop BCS corrections to the exchange interaction g_1, and the inter-band Hubbard interaction g_2, as shown in Fig. 4. The first diagram in panel (a) illustrates a correction to the exchange interaction g_1. This correction involves two g_5 interactions. This diagram features two internal solid lines moving in the same direction, which are evaluated to be the negative BCS susceptibility, $-\chi_{pp}^{intra}$, from the first band. Similarly, the second diagram has two $-g_5$ interaction lines and a negative BCS susceptibility from the second band. These two diagrams thus add up to $\Delta g_1 = -2\chi_{pp}^{intra} g_5^2$

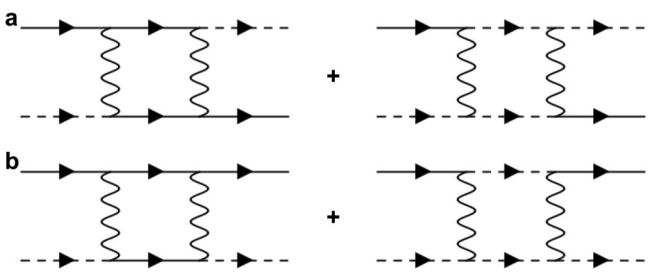

Fig. 4 | g_5-interaction leads to intra-band particle-particle corrections. (**a**) The correction to g_1. (**b**) The correction to g_2.

in Eq.(7). The two diagrams in panel (b) add up to $\Delta g_2 = -2\chi_{pp}^{intra} g_5^2$. Within BCS corrections, g_5 does not affect $g_{3,4}$.

Notably, these corrections are always negative, regardless of the signs of interactions. This can drive $g_{1,2} < 0$. In the appendix, we consider a patch renormalization group study including subleading corrections, which are important as $g_4 - g_3$ vanish[81]. We consider the small $g_{3,4}$ sector and explicitly show that BCS corrections from g_5 can push the RG flow to stable fixed points with divergent $g_{1,2} < 0$.

Competing instabilities

The above discussion reveals that negative g_1 and g_2 can become the dominant interactions, and so we may neglect other interactions. We find that g_1 and g_2 generically lead to competing instabilities in the intra-band particle–hole, inter-band particle-hole, and inter-band particle-particle channels (Table 2). These instabilities are obtained from self-consistent one-loop vertex corrections in the appendix, and here are illustrated from a mean-field perspective. Specifically, d-wave altermagnetism $\tilde{\tau}_z\sigma$ requires an antiferromagnetic interaction between the two bands, which is contributed by the attractive inter-band Hubbard interaction g_2 (marked in blue below):

$$\begin{aligned}
S_{1z}S_{2z} &= (n_{1\uparrow} - n_{1\downarrow})(n_{2\uparrow} - n_{2\downarrow})\\
&= -(n_{1\uparrow}n_{2\downarrow} + n_{2\uparrow}n_{1\downarrow}) + n_{1\uparrow}n_{2\uparrow} + n_{1\downarrow}n_{2\downarrow}
\end{aligned} \tag{8}$$

The altermagnetism is in the intra-band particle-hole channel, so the instability criteria is $\chi_{ph}^{intra}|g_2|>1$, as shown in Table 2. Other instabilities include inter-band d_{xy} superconductivity, ϵ_{xy} nematicity, and orbital altermagnetic order. These order parameters inherit non-trivial symmetries through the band degrees of freedom $\tilde{\tau}_i$, even though the coincident Van Hove singularity is located at a single momentum point. The orbital altermagnetic order $\tilde{\tau}_y$ is a current-loop order breaking time-reversal symmetry while preserving all crystal reflection symmetries (Fig. 1). This state will induce an anomalous Hall effect under the application of an ϵ_{xy} strain, even without the presence of SOC (a detailed explanation is in the appendix). When SOC is present, this current loop order and the conventional d-wave spin altermagnetic order $\tilde{\tau}_z\sigma_z$ will coexist as these two orders share the same symmetry. It is notable that the d-wave superconductivity we find is inter-band, and cannot be stabilized through a conventional BCS mechanism.

While the one-loop correction for the interaction comes from the dominant intra-band particle-particle (BCS) channel, the one-loop correction for the vertices all belong to the three subleading channels. The ultimate leading instability can be determined by the magnitude of the three eigenvalues $\chi_{pp}^{inter}|g_1+g_2|$, $\chi_{ph}^{inter}|g_1|$ and $\chi_{ph}^{intra}|g_2|$. The three susceptibilities share the same scaling: $\chi \propto \log\Lambda_i/T$, generically with different energy cutoff Λ_i. To examine what parameter range enables the different instabilities, we set the cutoffs in all three susceptibilities the same and consider the limit $g_1 = g_2$. This limit occurs when only BCS corrections from on-site Coulomb interactions are included but generally $g_1 \neq g_2$. The results then depend upon the kp dispersion in Eq.(3). Figure 5 reveals that all instability channels are stable for some choice

Table 2 | Orders stabilized by coincident Van Hove points and corresponding symmetries and eigenvalues

Instability	Eigenvalue
d-wave altermagnetism: $\tilde{\tau}_z\sigma \sim k_xk_y\sigma$	$\chi_{ph}^{intra}\|g_2\|$
Nematicity: $\tilde{\tau}_x \sim k_xk_y$	$\chi_{ph}^{inter}\|g_1\|$
Orbital altermagnetism: $\tilde{\tau}_y$	$\chi_{ph}^{inter}\|g_1\|$
d-wave SC: $\tilde{\tau}_x(i\sigma_y) \sim k_xk_y(i\sigma_y)$	$\chi_{pp}^{inter}\|g_1+g_2\|$

https://doi.org/10.1038/s41467-025-57970-9

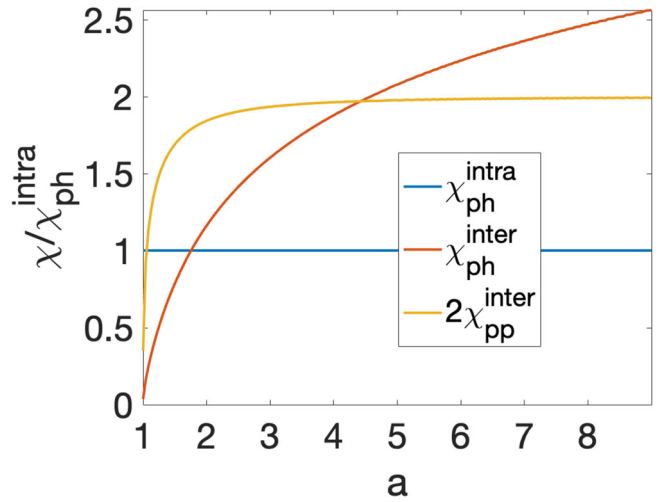

Fig. 5 | Susceptibilities χ_{pp}^{inter}, χ_{ph}^{inter} and χ_{ph}^{intra}, normalized with respect to χ_{ph}^{intra}, with $t_x = t_y$ and $a \equiv \frac{\sqrt{t_4^2+t_5^2}}{2t_x}$. $2\chi_{pp}^{inter}$ is plotted as the SC vertex is contributed by both g_1 and g_2. $N = 2000^2$ points are sampled, for $k_{x,y} \in [-5, 5]$. Temperature $T/t_x = 0.01$ is taken. $\mathbf{q} = (10^{-4}, 0)$ is used in χ_{ph}^{intra}. $\mathbf{q} = (0, 0)$ is used in χ_{ph}^{inter} and χ_{pp}^{inter}.

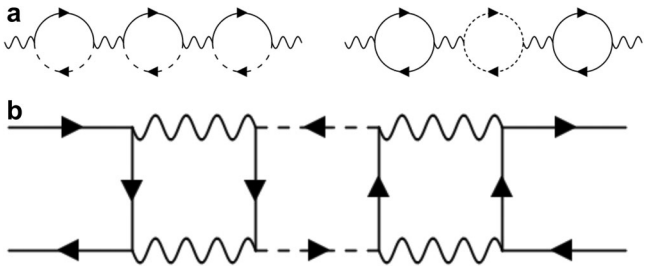

Fig. 6 | Comparison of conventional and the g_5 bubbles to magnetism. **a** Conventional Stoner bubbles from $g_{1,2}$, for intra-band and inter-band particle-hole channel. **b** Contribution through intra-band particle-particle channel from the g_5 interaction. The two pairs of vertical propagators can be from both patches.

of $a \equiv \frac{\sqrt{t_4^2+t_5^2}}{2t_x}$ (Van Hove dispersion requires $a > 1$). We note that once $g_1 > g_2$ (or $g_1 < g_2$), the inter-band (or intra-band) altermagnetic phase will expand.

It is worth noting that the above results are not captured by the standard random phase approximation (RPA). The RPA diagram is shown in panel (a) in Fig. 6. It gives the usual instability criteria $|g_2|\chi_{ph}^{intra} > 1$ (topleft) and $|g_1|\chi_{ph}^{inter} > 1$ (topright). The BCS instability for altermagnetism is equivalent to a two-loop correction described by panel (b). This diagram is derived from panel (a) by substituting the g_2 interaction with its g_5-correction in Fig. 4. The instability criteria is thus $|\Delta g_2|\chi_{ph}^{intra} = 2|g_5|^2\chi_{pp}^{intra}\chi_{ph}^{intra} > 1$. Since $\chi_{pp}^{intra} \gg \chi_{ph}^{intra}, \chi_{ph}^{inter}$ at low temperature, the BCS correction from g_5 describes a stronger weak-coupling instability. Since the g_5 contributions exceed the RPA-based contributions in the weak-coupling limit, it is reasonable to include them beyond the conventional RPA-based contributions when addressing intermediate and strong coupling problems in future studies.

Our coincident Van Hove mechanism relies on the existence of a g_5 hopping interaction and exclusively yields d-wave altermagnetic states. Given the discovery of g-wave altermagnetism[82,83], it is interesting to ask if there exists a weak-coupling Van Hove scenario that stabilizes such a g-wave state. In the appendix we show that this is indeed possible for a different coincident Van Hove scenario that also applies to many of the space groups examined here. In this case, a momentum-dependent spin-splitting of the form $k_x k_y(k_x^2 - k_y^2)$ is generated from coincident Van Hove singularities with a symmetry that forbid the existence of the g_5 interaction. This Van Hove scenario can be mapped onto the patch model for the cuprates[59] and this mapping reveals that the Neel spin density wave state found for the cuprate case maps to the g-wave altermagnetic state. In contrast to the d-wave altermagnetic that appears when $g_5 \neq 0$, the g-wave altermagnetic state requires nesting to become stable.

Group theory arguments

We now explicitly derive the symmetry requirements that underlie the kp Hamiltonian in Eq.(2). Key to this argument are non-symmorphic 2-fold symmetries. For these symmetries, we adopt the notation $\widetilde{O} = \{O|\mathbf{t}\}$ to describe a reflection symmetry O followed by a half-translation vector $\mathbf{t}$. We also denote a pure translation as $\{t^x, t^y\}$. The first requirement for Eq.(2) is a 2-fold sublattice degeneracy, which appears independently of 2-fold spin degeneracy. This degeneracy is ensured by the product of spinless time-reversal symmetry T (here T is represented by the complex conjugation operator) and a non-symmorphic symmetry. For example in κ-Cl, reflection symmetry $\widetilde{M}_x = \{M_x|1/2, 1/2\}$ takes the position (x, y) to $(-x + 1/2, y + 1/2)$. We have $(T\widetilde{M}_x)^2 = -1$, which follows for $T^2 = 1$ and $(\widetilde{M}_x)^2 = \{0, 1\} = \exp(ik_y)$ when the momentum of the Bloch state has $k_y = \pi$. The TRIM point thus exhibits 2-fold sublattice degeneracy. In this work, we do not consider TRIM points with higher sublattice degeneracies.

As the T invariant operators τ_x and τ_z both share the same non-trivial transformation properties as $k_x k_y$, this places the second constraint on possible allowed little co-groups (the group of crystal symmetries that keep the relevant momentum point unchanged up to a reciprocal lattice vector). Specifically, the little co-group must have a specific irreducible representation that transforms as $k_x k_y$. This representation should not mix in other quadratic terms, such as k_x^2, because that would lead to terms like $k_x^2\tau_x$ in the kp Hamiltonian. Notably, linear terms like $k_x\tau_x$ are already excluded from the kp Hamiltonian by T.

Now suppose $\tau_{x,z}$ already transform as $k_x k_y$. Since τ_y is proportional to the product of τ_x and τ_z, it must transform trivially under all crystal symmetries, and belong to the trivial representation. The trivial representation should not mix in linear terms like k_x, because that would lead to terms like $k_x\tau_y$ in the Hamiltonian.

Let us check the above requirements of little co-groups on κ-Cl, which has mirror symmetries $\widetilde{M}_x = \{M_x|1/2, 1/2\}$, $\widetilde{M}_y = \{M_y|1/2, 1/2\}$, and their product C_{2z}. These three symmetries keep the TRIM point (π, π) invariant. At this TRIM point, these symmetries form the 2mm point group. In this point group, the A_2 representation only hosts $k_x k_y$ at quadratic level. The trivial A_1 representation does not contain k-odd terms in (k_x, k_y). The above requirement of little co-groups are thus satisfied.

The third requirement is on the symmetry operators. Because T commutes with all crystal symmetries, these symmetries are represented by real 2×2 matrices. Since τ_y is invariant under all crystal symmetries, these matrices should commute with τ_y. Hence, they are either $\pm\tau_0$(identity) or $\pm i\tau_y$. This implies that all the symmetry operators at the TRIM point should commute with each other.

If a symmetry preserves $\tau_{x,z} \sim k_x k_y$, then $\tau_{x,z}$ should commute with the symmetry matrix. The symmetry operator is then $\pm\tau_0$. Such symmetries are thus squared to $+1$. If a symmetry flips $k_x k_y$, then $\tau_{x,z}$ should anticommute with the symmetry matrix. The symmetry matrix is then $\pm i\tau_y$. Such symmetries are thus squared to -1.

We can now deduce the remaining symmetry requirements for the kp Hamiltonian in Eq.(2): (1) All the symmetry operators at the TRIM point commute with each other. (2) Symmetries preserving $k_x k_y$

are squared to +1 while symmetries flipping k_xk_y are squared to −1. As shown below, these requirements can be checked without explicitly introducing matrix representations for the symmetries.

Let us check the above requirements for the symmetries on κ-Cl. Firstly, $\widetilde{M_x}$ and $\widetilde{M_y}$ commute as:

$$\begin{aligned}&\{M_x|t_x^x,t_x^y\}\{M_y|t_y^x,t_y^y\}\\&=\{-2t_y^x,2t_x^y\}\{M_y|t_y^x,t_y^y\}\{M_x|t_x^x,t_x^y\}\\&=\{-1,1\}\{M_y|t_y^x,t_y^y\}\{M_x|t_x^x,t_x^y\}\end{aligned}\tag{9}$$

In real space, the commutator is evaluated into a translation operation $\{-1,1\}$, which is equal to +1 at the $(k_x,k_y)=(\pi,\pi)$ point. Symmetries $\widetilde{M_x}$, $\widetilde{M_y}$, and their product C_{2z} thus commute with each other.

Note that k_xk_y is odd under $\widetilde{M_x}$ and $\widetilde{M_y}$, but even under their product C_{2z}. Consequently, we require $\widetilde{M_x}^2=\widetilde{M_y}^2=-1$, and $C_{2z}^2=+1$. To check this:

$$\begin{aligned}\widetilde{M_x}^2&=\{0,1\}=\exp(ik_y)=-1\\\widetilde{M_y}^2&=\{1,0\}=\exp(ik_x)=-1\\C_{2z}^2&=\{0,0\}=1.\end{aligned}\tag{10}$$

The symmetry conditions are thus satisfied in κ-Cl. Table 1 is obtained by checking the above three requirements for TRIM points in all 2D layer groups and 3D space groups.

Discussion

Here we have identified coincident Van Hove singularities as a platform to realize 2D altermagnetic states and other novel electronic states. These states are stabilized due to a new interaction term, g_5, through a weak-coupling BCS mechanism that leads to altermagnetism, nematic, d-wave superconducting, and orbital altermagnetic orders. Our results apply to nine 2D space groups and we have chosen a specific application in κ-Cl, where altermagnetism with the same symmetry found here is observed in κ-Cl[84] and d-wave superconductivity is reported under pressure[64,65] and anion substitution[67–74]. Another relevant 2D material is monolayer RuF_4 in layer group L17(p2_1/b11). It has the same kp Hamiltonian as κ-Cl at the (π,π) point, and recent DFT calculation[85] reveals an altermagnetic instability within an RPA-like approach.

Although our study focuses on 2D systems, the same coincident Van Hove singularities exist at high symmetry momenta in the 3D space groups listed in Table 1. Strictly speaking, in 3D, there is no divergence in the density of states near the Van Hove singularity. However, the density of states can still be large near the Van Hove momentum in the quasi-2D limit. In this case, the BCS weak-coupling instability will still aid in stabilizing the altermagnetic states. Among these 3D space groups, 55(Pbam), 58(Pnnm), 62(Pnma), 136(P4_2/mnm), and 138(P4_2/ncm) are known to host multiple altermagnetic candidates, according to the search on MAGNDATA database[86]. In these 3D materials, the contribution of the coincident Van Hove singularity to the ordering instability can be revealed by studying the doping dependence of the altermagnetic transition temperature.

Data availability

All study data are included in the article and/or SI Appendix.

Code availability

Codes are available at https://doi.org/10.5281/zenodo.10994906.

References

1. Naka, M. et al. Spin current generation in organic antiferromagnets. *Nat. Commun.* **10**, 4305 (2019).
2. Šmejkal, L., González-Hernández, R., Jungwirth, T. & Sinova, J. Crystal time-reversal symmetry breaking and spontaneous hall effect in collinear antiferromagnets. *Sci. Adv.* **6**, eaaz8809 (2020).
3. Šmejkal, L., Sinova, J. & Jungwirth, T. Emerging research landscape of altermagnetism. *Phys. Rev. X* **12**, 040501 (2022).
4. Šmejkal, L., Sinova, J. & Jungwirth, T. Beyond conventional ferromagnetism and antiferromagnetism: A phase with nonrelativistic spin and crystal rotation symmetry. *Phys. Rev. X* **12**, 031042 (2022).
5. Noda, Y., Ohno, K. & Nakamura, S. Momentum-dependent band spin splitting in semiconducting MnO_2: a density functional calculation. *Phys. Chem. Chem. Phys.* **18**, 13294–13303 (2016).
6. Ahn, K.-H., Hariki, A., Lee, K.-W. & Kuneš, J. Antiferromagnetism in RuO_2 as d-wave Pomeranchuk instability. *Phys. Rev. B* **99**, 184432 (2019).
7. Hayami, S., Yanagi, Y. & Kusunose, H. Momentum-dependent spin splitting by collinear antiferromagnetic ordering. *J. Phys. Soc. Jpn.* **88**, 123702 (2019).
8. Hayami, S., Yanagi, Y. & Kusunose, H. Bottom-up design of spin-split and reshaped electronic band structures in antiferromagnets without spin-orbit coupling: procedure on the basis of augmented multipoles. *Phys. Rev. B* **102**, 144441 (2020).
9. Yuan, L.-D., Wang, Z., Luo, J.-W. & Zunger, A. Prediction of low-z collinear and noncollinear antiferromagnetic compounds having momentum-dependent spin splitting even without spin-orbit coupling. *Phys. Rev. Mater.* **5**, 014409 (2021).
10. Mazin, I. I., Koepernik, K., Johannes, M. D., González-Hernández, R. & Šmejkal, L. Prediction of unconventional magnetism in doped $FeSb_2$. *Proc. Natl Acad. Sci.* **118**, e2108924118 (2021).
11. Berlijn, T. et al. Itinerant antiferromagnetism in RuO_2. *Phys. Rev. Lett.* **118**, 077201 (2017).
12. Zhu, Z. H. et al. Anomalous antiferromagnetism in metallic RuO_2 determined by resonant x-ray scattering. *Phys. Rev. Lett.* **122**, 017202 (2019).
13. Kivelson, S. A. et al. How to detect fluctuating stripes in the high-temperature superconductors. *Rev. Mod. Phys.* **75**, 1201 (2003).
14. Šmejkal, L., MacDonald, A. H., Sinova, J., Nakatsuji, S. & Jungwirth, T. Anomalous hall antiferromagnets. *Nat. Rev. Mater.* **7**, 482–496 (2022).
15. Feng, Z. et al. An anomalous Hall effect in altermagnetic ruthenium dioxide. *Nat. Electron.* **5**, 735–743 (2022).
16. Betancourt, R. D. et al. Spontaneous anomalous Hall effect arising from an unconventional compensated magnetic phase in a semiconductor. *Phys. Rev. Lett.* **130**, 036702 (2023).
17. Naka, M. et al. Anomalous Hall effect in κ-type organic antiferromagnets. *Phys. Rev. B* **102**, 075112 (2020).
18. Nakatsuji, S., Kiyohara, N. & Higo, T. Large anomalous Hall effect in a non-collinear antiferromagnet at room temperature. *Nature* **527**, 212–215 (2015).
19. Samanta, K. et al. Crystal Hall and crystal magneto-optical effect in thin films of $SrRuO_3$. *J. Appl. Phys.* **127** (2020).
20. Sürgers, C., Kittler, W., Wolf, T. & Löhneysen, H. V. Anomalous hall effect in the noncollinear antiferromagnet Mn_5Si_3. *AIP Adv.* **6** (2016)
21. Ghimire, N. J. et al. Large anomalous Hall effect in the chiral-lattice antiferromagnet $CoNb_3S_6$. *Nat. Commun.* **9**, 3280 (2018).
22. Jungwirth, T., Marti, X., Wadley, P. & Wunderlich, J. Antiferromagnetic spintronics. *Nat. Nanotechnol.* **11**, 231–241 (2016).
23. Šmejkal, L., Hellenes, AnnaBirk, González-Hernández, R., Sinova, J. & Jungwirth, T. Giant and tunneling magnetoresistance in unconventional collinear antiferromagnets with nonrelativistic spin-momentum coupling. *Phys. Rev. X* **12**, 011028 (2022).
24. Hariki, A. et al. X-ray magnetic circular dichroism in altermagnetic α-mnte. *Phys. Rev. Lett.* **132**, 176701 (2024).
25. Yuan, L.-D., Wang, Z., Luo, J.-W., Rashba, E. I. & Zunger, A. Giant momentum-dependent spin splitting in centrosymmetric low-z antiferromagnets. *Phys. Rev. B* **102**, 014422 (2020).

26. González-Hernández, R. et al. Efficient electrical spin splitter based on nonrelativistic collinear antiferromagnetism. *Phys. Rev. Lett.* **126**, 127701 (2021).
27. Naka, M., Motome, Y. & Seo, H. Perovskite as a spin current generator. *Phys. Rev. B* **103**, 125114 (2021).
28. Shao, D.-F., Zhang, S.-H., Li, M., Eom, C.-B. & Tsymbal, E. Y. Spin-neutral currents for spintronics. *Nat. Commun.* **12**, 7061 (2021).
29. Bose, A. et al. Tilted spin current generated by the collinear antiferromagnet ruthenium dioxide. *Nat. Electron.* **5**, 267–274 (2022).
30. Ma, H.-Y. et al. Multifunctional antiferromagnetic materials with giant piezomagnetism and noncollinear spin current. *Nat. Commun.* **12**, 2846 (2021).
31. Guo, S.-D., Guo, X.-S., Cheng, K., Wang, K. & Ang, Y. S. Piezoelectric altermagnetism and spin-valley polarization in Janus monolayer Cr_2So. *Appl. Phys. Lett.* **123** (2023)
32. Steward, C. R. W., Fernandes, R. M. & Schmalian, J. örg Dynamic paramagnon-polarons in altermagnets. *Phys. Rev. B* **108**, 144418 (2023).
33. Liu, Z. Q. et al. Electrical switching of the topological anomalous hall effect in a non-collinear antiferromagnet above room temperature. *Nat. Electron.* **1**, 172–177 (2018).
34. López-Moreno, Sinhué, Romero, A. H., Mejía-López, J., Muñoz, A. & Roshchin, I. V. First-principles study of electronic, vibrational, elastic, and magnetic properties of FeF_2 as a function of pressure. *Phys. Rev. B* **85**, 134110 (2012).
35. Karube, S. et al. Observation of spin-splitter torque in collinear antiferromagnetic RuO_2. *Phys. Rev. Lett.* **129**, 137201 (2022).
36. Bai, H. et al. Observation of spin splitting torque in a collinear antiferromagnet RuO_2. *Phys. Rev. Lett.* **128**, 197202 (2022).
37. Tomczak, J. M. Thermoelectricity in correlated narrow-gap semiconductors. *J. Phys.: Condens. Matter* **30**, 183001 (2018).
38. Zhou, X. et al. Crystal thermal transport in altermagnetic RuO_2. *Phys. Rev. Lett.* **132**, 056701 (2024).
39. Papaj, M. Andreev reflection at altermagnet/superconductor interface. *Phys. Rev. B.* **108**, L060508 (2023).
40. Beenakker, C. W. J. & Vakhtel, T. Phase-shifted Andreev levels in an altermagnet Josephson junction. *Phys. Rev. B* **108**, 075425 (2023).
41. Zhu, D., Zhuang, Z.-Y., Wu, Z. & Yan, Z. Topological superconductivity in two-dimensional altermagnetic metals. *Phys. Rev. B* **108**, 184505 (2023).
42. Zhang, S.-B., Hu, L.-H. & Neupert, T. Finite-momentum cooper pairing in proximitized altermagnets. *Nat. Commun.* **15**, 1801 (2024).
43. Sumita, S., Naka, M. & Seo, H. Fulde-ferrell-larkin-ovchinnikov state induced by antiferromagnetic order in κ-type organic conductors. *Phys. Rev. Res.* **5**, 043171 (2023).
44. Ghorashi, S. A. A., Hughes, T. L. & Cano, J. Altermagnetic routes to Majorana modes in zero net magnetization. *Phys. Rev. Lett.* **133**, 106601 (2024).
45. Roig, M., Kreisel, A., Yu, Y., Andersen, B. M. & Agterberg, D. F. Minimal models of altermagnetism. *Phys. Rev. B.* **110**, 144412 (2024).
46. Wu, C., Sun, K., Fradkin, E. & Zhang, S.-C. Fermi liquid instabilities in the spin channel. *Phys. Rev. B* **75**, 115103 (2007).
47. Kiesel, M. L., Platt, C., Hanke, W., Abanin, D. A. & Thomale, R. Competing many-body instabilities and unconventional superconductivity in graphene. *Phys. Rev. B* **86**, 020507 (2012).
48. Nandkishore, R., Levitov, L. S. & Chubukov, A. V. Chiral superconductivity from repulsive interactions in doped graphene. *Nat. Phys.* **8**, 158–163 (2012).
49. Wang, W.-S. et al. Functional renormalization group and variational Monte Carlo studies of the electronic instabilities in graphene near 1 4 doping. *Phys. Rev. B* **85**, 035414 (2012).
50. Furukawa, N., Rice, T. M. & Salmhofer, M. Truncation of a two-dimensional fermi surface due to quasiparticle gap formation at the saddle points. *Phys. Rev. Lett.* **81**, 3195 (1998).
51. Kampf, A. P. & Katanin, A. A. Competing phases in the extended U–V–J Hubbard model near the van Hove fillings. *Phys. Rev. B* **67**, 125104 (2003).
52. Honerkamp, C., Salmhofer, M., Furukawa, N. & Rice, T. M. Breakdown of the Landau-Fermi liquid in two dimensions due to umklapp scattering. *Phys. Rev. B* **63**, 035109 (2001).
53. Le Hur, K. & Rice, T. M. Superconductivity close to the Mott state: from condensed-matter systems to superfluidity in optical lattices. *Ann. Phys.* **324**, 1452–1515 (2009).
54. Wang, W.-S., Li, Z.-Z., Xiang, Y.-Y. & Wang, Q.-H. Competing electronic orders on kagome lattices at van hove filling. *Phys. Rev. B* **87**, 115135 (2013).
55. Gonzalez, J. Kohn-Luttinger superconductivity in graphene. *Phys. Rev. B* **78**, 205431 (2008).
56. Martin, I. & Batista, C. D. Itinerant electron-driven chiral magnetic ordering and spontaneous quantum hall effect in triangular lattice models. *Phys. Rev. Lett.* **101**, 156402 (2008).
57. Halboth, C. J. & Metzner, W. Renormalization-group analysis of the two-dimensional Hubbard model. *Phys. Rev. B* **61**, 7364 (2000).
58. Honerkamp, C. & Salmhofer, M. Temperature-flow renormalization group and the competition between superconductivity and ferromagnetism. *Phys. Rev. B* **64**, 184516 (2001).
59. Schulz, H. J. Superconductivity and antiferromagnetism in the two-dimensional Hubbard model: Scaling theory. *Europhys. Lett.* **4**, 609 (1987).
60. Kiesel, M. L. & Thomale, R. Sublattice interference in the Kagome Hubbard model. *Phys. Rev. B* **86**, 121105 (2012).
61. Yu, S.-L. & Li, J.-X. Chiral superconducting phase and chiral spin-density-wave phase in a Hubbard model on the kagome lattice. *Phys. Rev. B* **85**, 144402 (2012).
62. Classen, L., Chubukov, A. V., Honerkamp, C. & Scherer, M. M. Competing orders at higher-order van Hove points. *Phys. Rev. B* **102**, 125141 (2020).
63. McKenzie, R. H. Similarities between organic and cuprate superconductors. *Science* **278**, 820–821 (1997).
64. Williams, J. M. et al. From semiconductor-semiconductor transition (42 K) to the highest-T_c organic superconductor. kappa.-(ET) 2Cu[N(CN)2]Cl (T_c= 12.5 K). *Inorg. Chem.* **29**, 3272–3274 (1990).
65. Miyagawa, K., Kanoda, K. & Kawamoto, A. Nmr studies on two-dimensional molecular conductors and superconductors: Mott transition in κ-(BEDT-TTF)2x. *Chem. Rev.* **104**, 5635–5654 (2004).
66. Kagawa, F., Miyagawa, K. & Kanoda, K. Unconventional critical behaviour in a quasi-two-dimensional organic conductor. *Nature* **436**, 534–537 (2005).
67. Kurosaki, Y., Shimizu, Y., Miyagawa, K., Kanoda, K. & Saito, G. Mott transition from a spin liquid to a fermi liquid in the spin-frustrated organic conductor κ-(ET)$2Cu_2(CN)_3$. *Phys. Rev. Lett.* **95**, 177001 (2005).
68. Miyagawa, K., Kawamoto, A. & Kanoda, K. Proximity of pseudogapped superconductor and commensurate antiferromagnet in a quasi-two-dimensional organic system. *Phys. Rev. Lett.* **89**, 017003 (2002).
69. Kanoda, K. Electron correlation, metal-insulator transition and superconductivity in quasi-2d organic systems, (ET)2x. *Phys. C: Supercond.* **282**, 299–302 (1997).
70. Mayaffre, H., Wzietek, P., Jérome, D., Lenoir, C. & Batail, P. Superconducting state of κ-(ET)2Cu[N(CN)2] br studied by C13 NMR: evidence for vortex-core-induced nuclear relaxation and unconventional pairing. *Phys. Rev. Lett.* **75**, 4122 (1995).
71. De Soto, S. M. et al. C13 NMR studies of the normal and superconducting states of the organic superconductor κ-(ET)2Cu[N(CN) 2]Br. *Phys. Rev. B* **52**, 10364 (1995).
72. Kanoda, K., Miyagawa, K., Kawamoto, A. & Nakazawa, Y. Nmr relaxation rate in the superconducting state of the organic conductor κ-(BEDT-TTF) 2Cu[N(CN)2]Br. *Phys. Rev. B* **54**, 76 (1996).

73. Urayama, H. et al. A new ambient pressure organic superconductor based on BEDT-TTF with T_c higher than 10 K (T_c = 10.4 K). *Chem. Lett.* **17**, 55–58 (1988).
74. Kini, A. M. et al. A new ambient-pressure organic superconductor. kappa.-(ET) 2Cu[N(CN)2]Br, with the highest transition temperature yet observed (inductive onset T_c = 11.6 K, resistive onset= 12.5 K). *Inorg. Chem.* **29**, 2555–2557 (1990).
75. Kuroki, K., Kimura, T., Arita, R., Tanaka, Y. & Matsuda, Y. d_{x2-y2}-versus d_{xy}-like pairings in organic superconductors κ-(BEDT-TTF) 2x. *Phys. Rev. B* **65**, 100516 (2002).
76. Sekine, A., Nasu, J. & Ishihara, S. Polar charge fluctuation and superconductivity in organic conductors. *Phys. Rev. B—Condens. Matter Mater. Phys.* **87**, 085133 (2013).
77. Guterding, D., Altmeyer, M., Jeschke, H. O. & Valentí, R. Near-degeneracy of extended s+ d_{x2-y2} and d_{xy} order parameters in quasi-two-dimensional organic superconductors. *Phys. Rev. B* **94**, 024515 (2016).
78. Koretsune, T. & Hotta, C. Evaluating model parameters of the κ-and β-type mott insulating organic solids. *Phys. Rev. B* **89**, 045102 (2014).
79. Kawasugi, Y. et al. Electron–hole doping asymmetry of fermi surface reconstructed in a simple Mott insulator. *Nat. Commun.* **7**, 12356 (2016).
80. Suh, HanGyeol et al. Superconductivity of anomalous pseudospin in nonsymmorphic materials. *Phys. Rev. Res.* **5**, 033204 (2023).
81. Arovas, D. P., Berg, E., Kivelson, S. A. & Raghu, S. The Hubbard model. *Annu. Rev. Condens. Matter Phys.* **13**, 239–274 (2022).
82. Krempasky`, J. et al. Altermagnetic lifting of Kramers spin degeneracy. *Nature* **626**, 517–522 (2024).
83. Mazin, I., González-Hernández, R. & Šmejkal, L. Induced monolayer altermagnetism in MnP (S, Se)$_3$ and FeSe. Preprint at https://arxiv.org/abs/2309.02355 (2023).
84. Miyagawa, K., Kawamoto, A., Nakazawa, Y. & Kanoda, K. Antiferromagnetic ordering and spin structure in the organic conductor, κ-(bedt-ttf) 2 cu [n (cn) 2] cl. *Phys. Rev. Lett.* **75**, 1174 (1995).
85. Milivojević, M., Orozović, M., Picozzi, S., Gmitra, M. & Stavrić, S. Interplay of altermagnetism and weak ferromagnetism in two-dimensional ruf4. *2D Mater.* **11**, 035025 (2024).
86. Guo, Y. et al. Spin-split collinear antiferromagnets: a large-scale ab-initio study. *Mater. Today Phys.* **32**, 100991 (2023).
87. de la Flor, G., Souvignier, B., Madariaga, G. & Aroyo, M. I. Layer groups: Brillouin-zone and crystallographic databases on the bilbao crystallographic server. *Acta Crystallogr. A: Found. Adv.* **77**, 559–571 (2021).
88. Kopsky`, V. & Litvin, D. B. International Tables for Crystallography. 2nd edn, Vol. E (Wiley, 2010).

Acknowledgements

The authors thank Philip Brydon, Andrey Chubukov, Tatsuya Shishidou, Stephen Wilson, and Michael Weinert for useful discussions. D.F.A. and Y.Y. were supported by the National Science Foundation Grant No. DMREF 2323857 (for one loop and patch RG calculations). D.F.A. and H.G.S. were supported by the Department of Energy, Office of Basic Energy Science, Division of Materials Sciences and Engineering under Award No. DE-SC0021971 (for the development of the symmetry-based Hamiltonians). M. R. acknowledges support from the Novo Nordisk Foundation grant NNF20OC0060019.

Author contributions

Y.Y., H.G.S., M.R., and D.F.A. designed research; performed research; contributed analytic tools; and wrote the paper.

Competing interests

The authors declare no competing interest.

Additional information

Supplementary information The online version contains supplementary material available at https://doi.org/10.1038/s41467-025-57970-9.

Correspondence and requests for materials should be addressed to Yue Yu.

Peer review information *Nature Communications* thanks the anonymous reviewer(s) for their contribution to the peer review of this work. A peer review file is available.